Mateos-Pérez, J. M.; Soto-Montenegro, M. L.; Peña-Zalbidea, S.; Desco, M.; Vaquero, J. J. (2016). "Functional segmentation of dynamic PET studies: Open source implementation and validation of a leader-follower-based algorithm". *Computers in Biology and Medicine*, v. 69, February, pp. 181-188.
DOI: 10.1016/j.compbiomed.2015.12.012

Supplementary Material File 2: visual results for the k-means algorithm.

Proyectos:
PI11/00616
PI14/ 00860
CPII/00005
TEC2014-56600-R
RETIC RD12/0042/0057
RGP0004/2013

We used a simulated study consisting of two cylinders with different levels of activity. These activity levels are described by the following equations:

$$C_{hot}(t)=\frac{k_1}{k_2}C_a+C_a(4-\frac{k_1}{k_2})e^{-k_2 t}$$

$$C_{cold}(t)=\frac{k_1}{k_2}C_a-C_a(\frac{k_1}{k_2})e^{-k_2 t}$$

In the previous equations, the constants are $k_1 = 0.01$ min^{-1}, $k_2 = 0.05$ min^{-1} for the hot cylinder; and $k_1 = 0.05$ min^{-1}, $k_2 = 0.01$ min^{-1} for the cold cylinder. C_a is a constant value of 12.4 μCi. An image of the phantom is shown on Figure 1; The matrix size is 175 x 175 x 61 voxels, with a voxel size of 1 mm x 1 mm x 2 mm. Twenty frames of 60 seconds each were simulated and reconstructed using an FBP algorithm. The theoretical curves are shown in Figure 2.

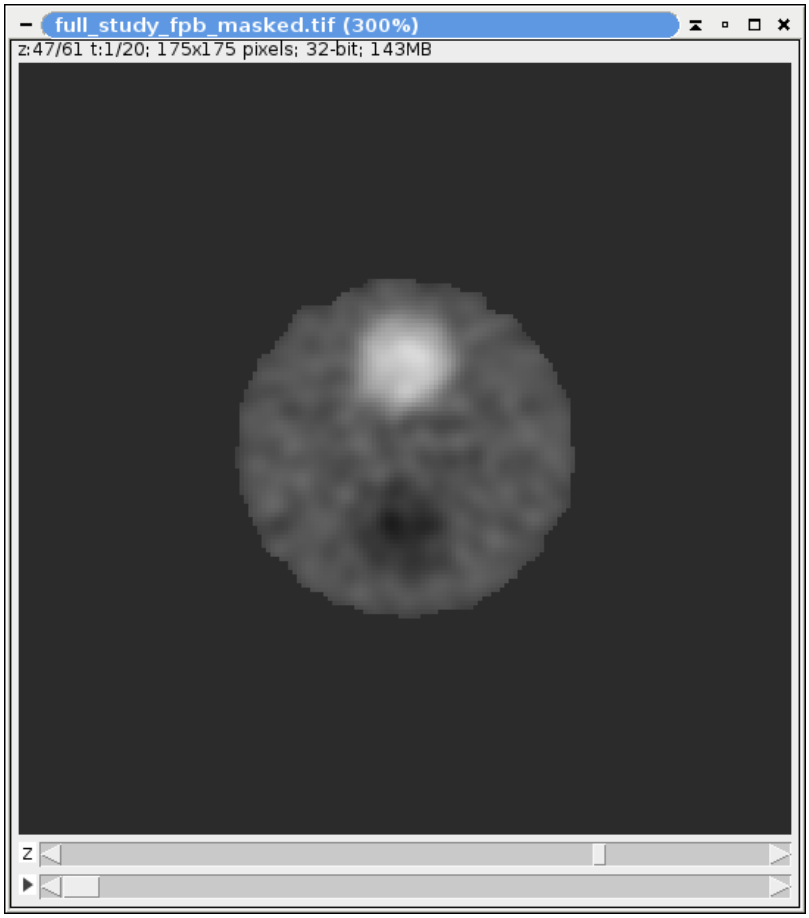

Figure 1: Phantom simulated in this study. The hot cylinder is located on the upper half of the container; the cold cylinder can be seen at the bottom.

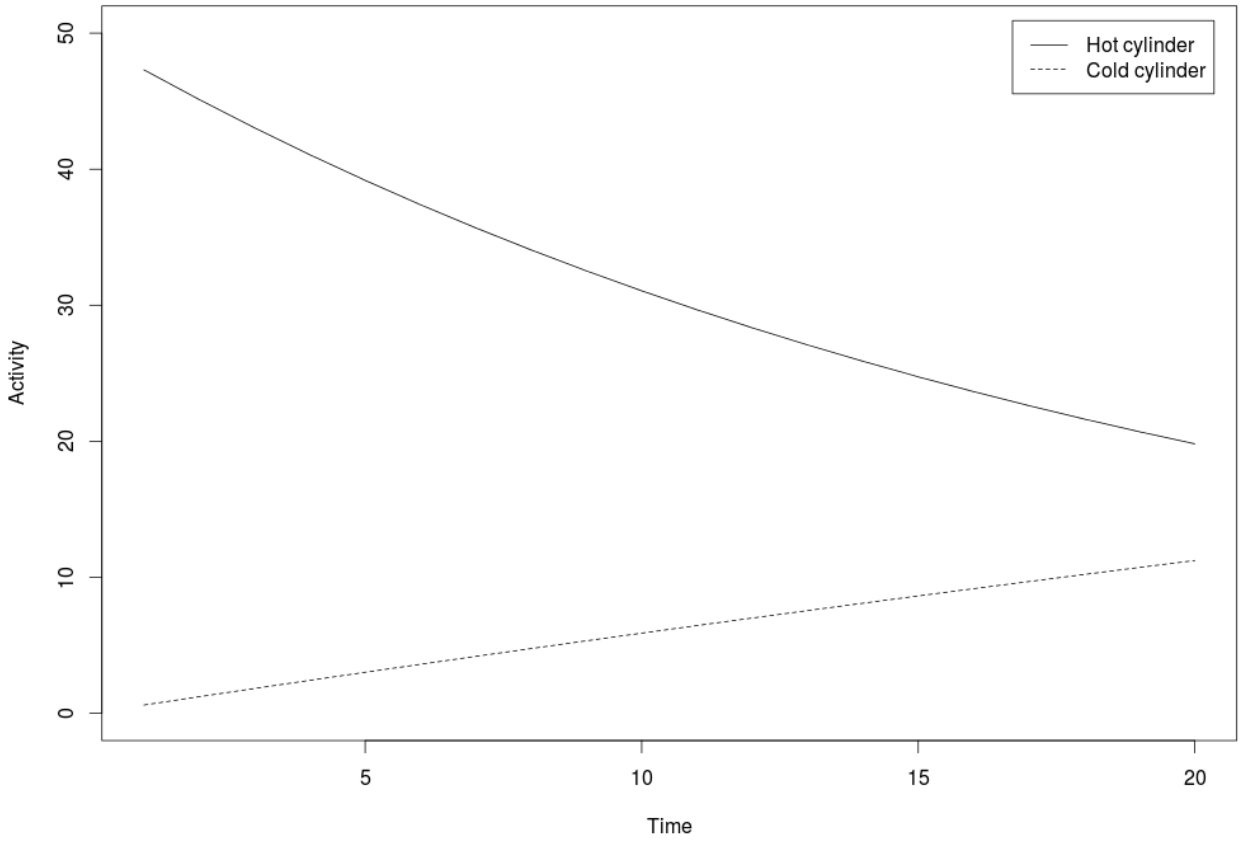

Figure 2: Theoretical activities for the phantom simulated in this study.

We performed two different segmentations over this phantom:

1. A manual segmentation, which was performed by placing small circular ROIs over a slice of the figure, centered on each of the cylinders and away from the borders in order to minimize partial volume effects.

2. An automatic segmentation with the proposed algorithm, using Pearson's correlation as the similarity metric with a threshold of 0.5.

Figure 3 shows the ROIs used during manual segmentation. Figure 4 shows the regions selected by the leader-follower algorithm.

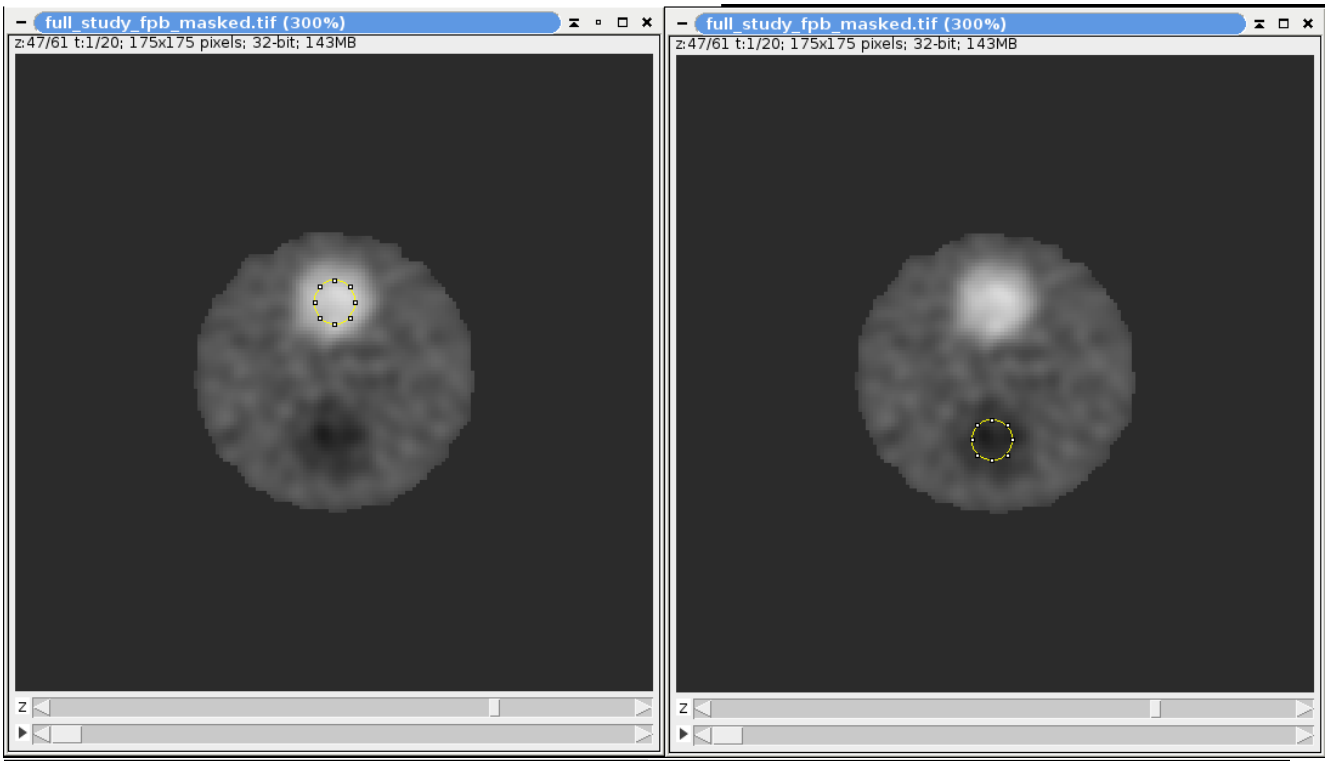

Figure 3: ROIs used for the automatic segmentation of the hot cylinder (left) and the cold cylinder (right).

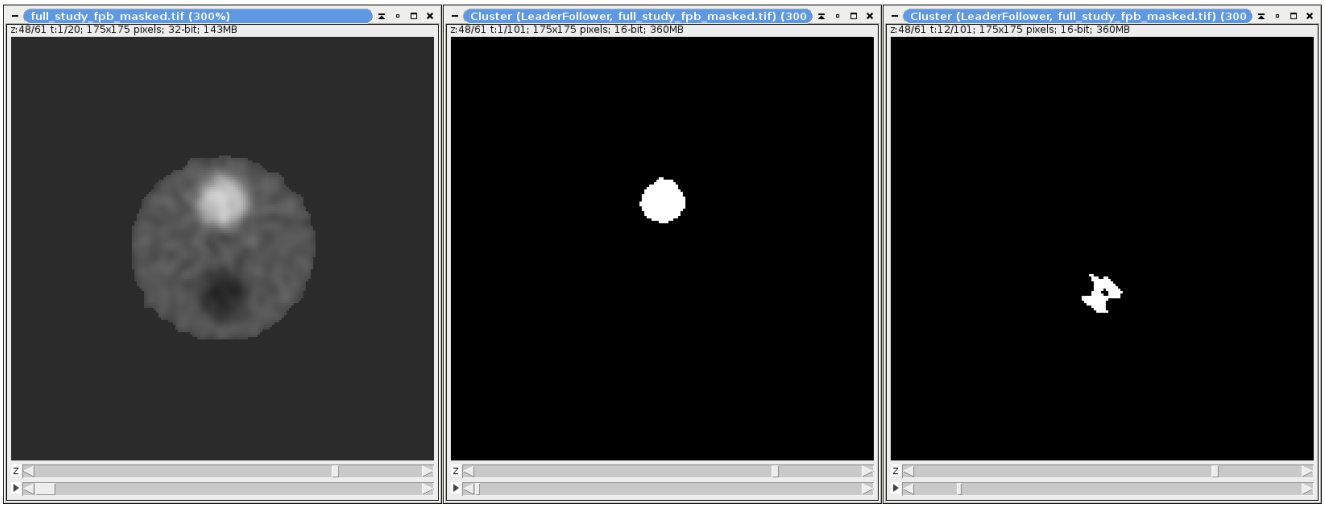

Figure 4: Regions selected for the automatic segmentation of the hot cylinder (center) and the cold cylinder (right). The same slice is shown on the leftmost panel for comparison purposes.

For this simulation, there is no calibration factor to convert AU from the reconstruction to concentration. AU was calculated directly from the data using a simple linear model (theoretical = factor * empirical). This operation is performed independently for both the automatic and the manual segmentation for comparison purposes.

Figure 5 shows the data once the empirical data have been calibrated.

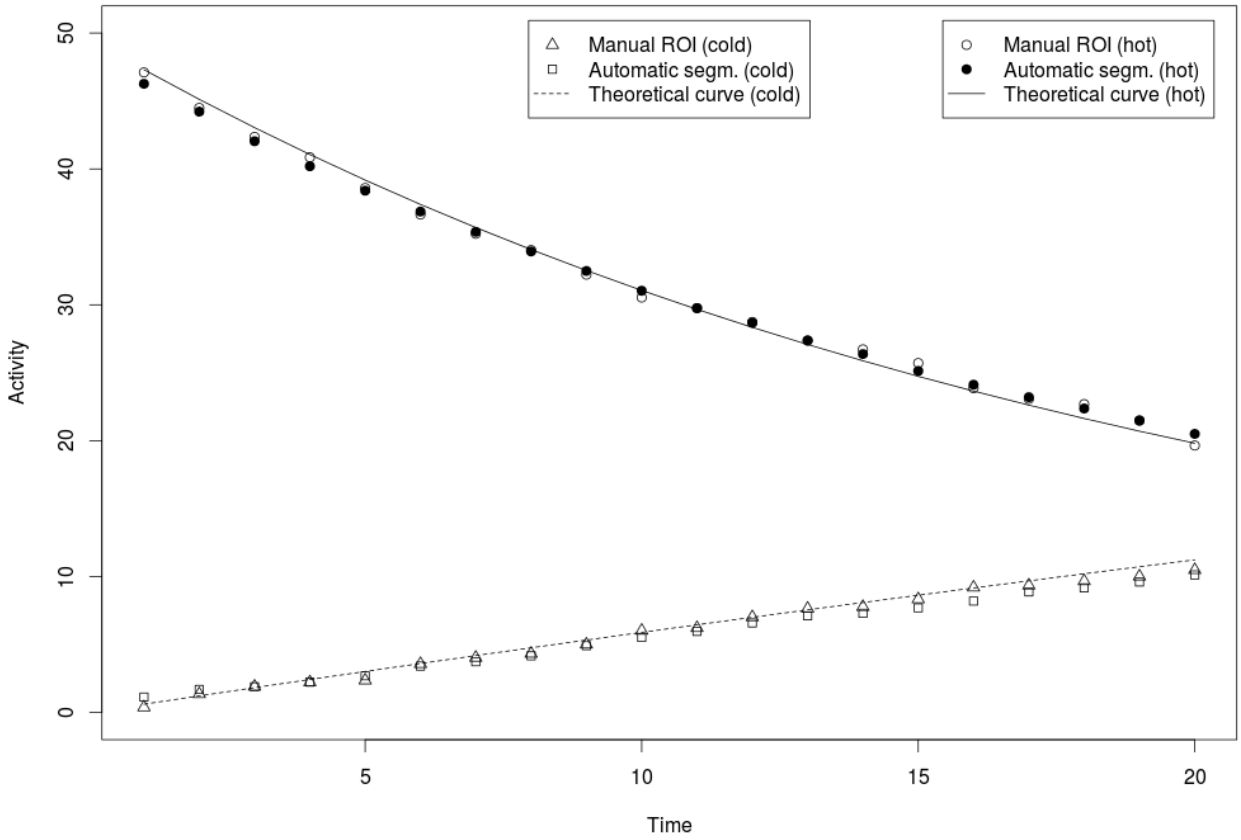

Figure 5: Calibrated empirical data. Automatic and manual curves are scaled with their corresponding calibration factors.

With this data calibrated, we can now proceed to the non-linear Levenberg-Marquardt algorithm in order to extract the k parameters from the automatic segmentation. The results can be seen in the following Table:

Method	Factor	*Hot* k_1	*Hot* k_2	*Cold* k_1	*Cold* k_2
Manual	3.832094	0.041 ± 20.3 %	0.061 ± 4.9 %	0.05 ± 3.4 %	0.014 ± 32 %
Automatic	4.121689	0.051 ± 14.6 %	0.064 ± 4.2 %	0.048 ± 3.1 %	0.017 ± 24 %

As can be seen, results differ from the theoretically expected ones for both the manual and the automatic results, especially in the case of the k_1 parameter for the hot cylinder. This can be explained in part because these simulations came from a study that characterized a reconstructor with a known bias that affects the slope of the signal as retrieved (Herranz, E., *"Formulación de modelos dinámicos de distribución temporal de fármacos en animales de laboratorio y contrastación con datos adquiridos en PET",* 2009). In any case, both segmentation techniques (automatic and manual) were shown to yield comparable results with a dataset other than that used in the main study presented.